Growth of ZnO nanostructures on Au-coated Si: Influence of growth temperature on growth mechanism and morphology

Kumar, Rajendra ; McGlynn, E.; Biswas, M.; Saunders, R.; Trolliard, G.; Soulestin, B.; Duclere, J.R.; Mosnier, J.P.; Henry, M.O.

Published in:
Journal of Applied Physics

Link to article, DOI:
10.1063/1.2996279

Publication date:
2008

Document Version
Publisher's PDF, also known as Version of record

Growth of ZnO nanostructures on Au-coated Si: Influence of growth temperature on growth mechanism and morphology

R. T. Rajendra Kumar,[1,2,a)] E. McGlynn,[1,a)] M. Biswas,[1] R. Saunders,[1] G. Trolliard,[3] B. Soulestin,[3] J.-R. Duclere,[3] J. P. Mosnier,[1] and M. O. Henry[1]
[1]*School of Physical Sciences, National Centre for Plasma Science and Technology (NCPST), Dublin City University, Glasnevin, Dublin 9, Ireland*
[2]*MIC-Department of Micro and Nanotechnology, Technical University of Denmark, DTU, Building 345 East, DK-2800 Kongens Lyngby, Denmark*
[3]*Laboratoire de Sciences des Procédés Céramiques et de Traitements de Surface, UMR 6638 CNRS, Université de Limoges, Faculté des Sciences, 123, avenue Albert Thomas, 87060 Limoges Cedex, France*

(Received 24 July 2008; accepted 20 August 2008; published online 24 October 2008)

ZnO nanostructures were grown on Au-catalyzed Si silicon substrates using vapor phase transport at growth temperatures from 800 to 1150 °C. The sample location ensured a low Zn vapor supersaturation during growth. Nanostructures grown at 800 and 850 °C showed a faceted rodlike morphology with mainly one-dimensional (1D) growth along the nanorod axis. Samples grown at intermediate temperatures (900, 950, and 1050 °C) in all cases showed significant three dimensional (3D) growth at the base of 1D nanostructures. At higher growth temperatures (1100 and 1150 °C) 3D growth tended to dominate resulting in the formation of a porous, nanostructured morphology. In all cases growth was seen only on the Au-coated region. Our results show that the majority of the nanostructures grow via a vapor-solid mechanism at low growth temperatures with no evidence of Au nanoparticles at their tip, in sharp contrast to the morphology expected for the vapor-liquid-solid (VLS) process often reported as the growth mechanism on Au-catalyzed Si. We see VLS growth only at 900 and 950 °C. Transmission electron microscopy data indicate that the nanorods are single crystalline without gross structural defects. Luminescence data reveal strong ultraviolet emission in all samples and weak defect emission in the visible region. We discuss the growth mechanisms with reference to various models in the literature and suggest reasons for VLS growth only in a narrow temperature range. We also discuss the potential effects of the Zn oxidation reaction on the growth morphologies, aspects largely ignored in the general literature on this subject. © *2008 American Institute of Physics*. [DOI: 10.1063/1.2996279]

I. INTRODUCTION

In recent years, tremendous effort has been devoted to the growth of ZnO nanostructures. ZnO possesses outstanding physical properties including a wide direct band gap, high excitonic binding energy, and high thermal and chemical stabilities which promise a range of applications in diverse areas such as ultraviolet (UV) lasing;[1] field emission displays,[2] resonators,[3] and sensors.[4] ZnO nanostructures of various morphologies are required for different applications. For example, well-aligned nanorods (NRs) appear to be best suited for field emitters and UV/white light emitting devices and nanowires appear optimally suited for applications as interconnects in nanoelectronic circuits and sensors. Understanding the growth process, and developing methods to control the morphology in a reasonably straightforward manner are vital aspects for commercial fabrication of ZnO nanostructures with various desired morphologies. ZnO nanostructures have been prepared using various techniques such as vapor phase transport[5] (VPT) chemical vapor deposition (CVD),[6] metal-organic CVD,[7] and chemical solution (CS) methods.[8] Among these techniques, the VPT method has been used extensively for growing ZnO nanostructures on metal catalyzed substrates, most commonly using Au as the catalyst.[9] In the case of metal catalyst-activated growth, where growth is seen solely on the metal-coated region, the growth mechanism is generally reported to be the vapor-liquid-solid (VLS) mechanism originally observed in Si whisker growth.[10] However, some more recent research work reports Au-catalyzed ZnO growth with features inconsistent with the VLS mechanism.[11,12] These reports indicate that the growth mechanism is vapor-solid (VS) growth.

In order to examine the various growth modes which operate in the 800–1150 °C temperature range we have undertaken a systematic study of growth of ZnO nanostructures on Au-catalyzed SiO_2/Si, where the SiO_2 is a native oxide layer. This temperature range is the most commonly used for VPT growth of ZnO nanostructures using carbothermal reduction in ZnO powder and spans the range from the onset of carbothermal reduction to the onset of direct ZnO congruent sublimation.[13,14] At all growth temperatures the growth proceeds at low Zn vapor supersaturation. In this regime the effects of the Au catalyst on the ZnO nanostructure nucleation are particularly important. We have also grown ZnO nanostructures on Au-catalyzed Si substrates which had a deliberately grown 3 μm thick SiO_2 layer.

[a)]Authors to whom correspondence should be addressed. Electronic addresses: rtrkumar@rediffmail.com and rajendra.kumar@nanotech.dtu.dk and enda.mcglynn@dcu.ie.

II. EXPERIMENTAL

ZnO nanostructures were grown on Au-catalyzed SiO_2/Si (001) substrates using the VPT technique. No effort is made to strip the native oxide prior to growth. For most growths Si substrates with native oxides were used, while a limited number of growths were made on thick (3 μm) on Si. The substrates were cleaned ultrasonically and a 5 nm Au layer was evaporated on the substrates in a bell jar evaporator. ZnO (99.999%)+carbon powders (99.9999%) at a 1:1 mass ratio were mixed and spread in an alumina boat. The substrates were then placed directly above the source powder on the boat with the growth surface facing the powder. This arrangement ensures low Zn vapor supersaturation.[15] We have used thermochemical tables to calculate the equilibrium concentration of Zn vapor over the range of temperatures used, based on the reaction in Eq. (1) in the later part of this paper, and to calculate the equilibrium Zn vapor pressure.[16–18] In order to calculate the Zn vapor supersaturation we have renormalized the total pressure in the chamber (i.e., including the background gas and the carbothermal reaction products) back to 1 atm, because the chamber is at atmospheric pressure due to the open end of the tube. We have then compared the renormalized Zn vapor pressure to the equilibrium Zn vapor pressure to calculate the Zn vapor supersaturation. A fuller account of this model with details of the free energy calculations will be published elsewhere. We take the sample temperature as being equal to the source material temperature, which is consistent with the experimental arrangement, described above, and is borne out by detailed measurements of the temperature profile of the furnace during growth. The resulting supersaturation levels vary between −1 and −0.7 and thus sticking/condensation of Zn atoms will only occur on regions of the substrate which have a high sticking coefficient for Zn vapor. The boat was placed in a quartz tube with an inner diameter of 37 mm and a length of ~1.2 m. The quartz tube is placed in a single zone tube furnace with the sample at the central portion of the furnace and a 90 SCCM (SCCM denotes cubic centimeter per minute at STP) Ar carrier gas flow was established through the tube. The other end of the tube is open to the external atmosphere. The gas flows for ~10 min prior to switching on the furnace and then the furnace temperature is set at various values from 800 to 1150 °C for different growths. The growth temperature is reached in ~15 min and the samples were grown for 30 min thereafter. We subsequently refer to different samples by the nominal growth temperature at which they were synthesized, though it must be borne in mind that the effects of the furnace ramp-up and cool-down times mean that each sample is exposed to a range of temperatures during the growth. However, the differences in the samples appear to be predominantly related to the differences in the nominal growth temperature. The growth products appear to the naked eye as a gray-white fog on the substrate when removed from the furnace. The details of the growth process are given in Refs. 5 and 19.

The microstructural and morphological properties of the samples were analyzed using x-ray diffraction (XRD; Bruker D8 Advance), scanning electron microscopy and high resolution scanning electron microscopy (SEM; LEO Steroscan 440: HR-SEM; Hitachi S-4300 Field Emission) and energy dispersive x-ray analysis (EDX; Princeton Gamma-Tech EDX spectrometer coupled to the LEO Stereoscan SEM).

The samples for transmission electron microscopy (TEM) analysis were prepared as follows. A piece of the silicon substrate with the Au layer covered by ZnO NR was immersed in a test tube filled with de-ionized water. The test tube was stirred in an ultrasonic bath for 10 min, followed by a 5 min resting period. A small quantity of the liquid was then collected and redeposited on a copper TEM grid, covered by a carbon membrane. The samples were finally dried. The microscope used is a JEOL 2010, operated with an acceleration voltage of 200 kV which also has an EDX capability. The camera length employed to record selected area electron diffraction (SAED) patterns is systematically equal to 100 cm.

Optical properties at room temperature were measured using cathodoluminescence (CL; Gatan Instruments Mono-CL coupled to the LEO Stereoscan SEM). The CL spectra were taken at a SEM magnification of 2000×, a voltage of 5 kV, a current of 1 nA, and a working distance of 15 mm in spot scan mode (i.e., fixing the electron beam on a spot and taking a CL spectrum). The CL data were collected from a region of $\sim 1 \times 1$ μm^2 in this mode. The resolution of the CL spectrometer was ~15 meV. Low temperature photoluminescence (PL) data were excited by the 325 nm line of a continuous wave HeCd laser (output power ~40 mW unfocused on the sample) and the spectra were measured using a Bomem DA8 FT spectrometer fitted with a Hamamatsu R1913 photomultiplier tube. The resolution of the spectrometer was ~0.5 meV in all cases, slightly less than the measured linewidths. Samples were cooled using a Janis CCS-500 closed-cycle cryostat and spectra were taken at ~18 K.

III. RESULTS AND DISCUSSION

A. Results

Si (001) substrates coated with 5 nm thick Au dots of ~2 mm diameter were used to grow ZnO nanostructures. It is found that ZnO nanostructures are only grown in the region where Au was deposited for all growth temperatures and no growth is observed either on uncoated areas of the Si substrate or using an uncatalyzed Si substrate. At higher temperatures (>1100 °C) the edges of the Au dots show some slight blurring and consequently ZnO growth takes place in this slightly larger region. This is due to diffusion effects for the Au, which have been reported previously for Si whisker growth.[10]

1. SEM

Figure 1 shows HR-SEM images displaying a top view at medium and high magnifications and a cross-sectional (*c*-section) view of ZnO nanostructures grown at 800, 850, 900, and 950 °C. In all cases the nanostructures grown show no evidence of preferential alignment perpendicular to the substrate as is the general case for growth on Si.[20]

Nanostructures grown at 800 °C [Figs. 1(a)–1(c)] are rodlike structures with length of 3–5 μm and diameters in

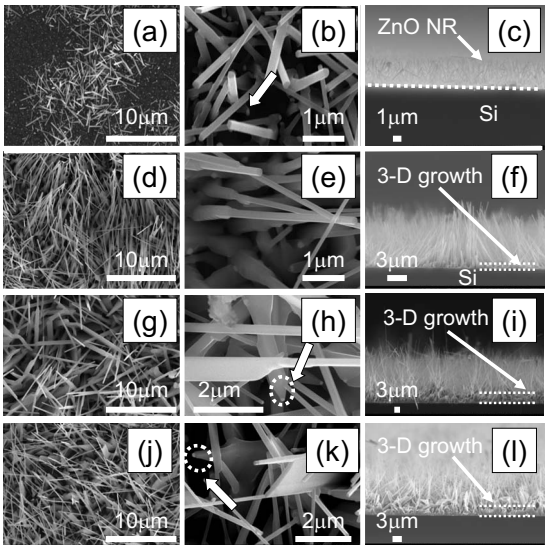

FIG. 1. HR-SEM images of ZnO nanostructures in plan view at low (5000×) and high (15 000–30 000×) magnifications and in cross-sectional view for samples grown at 800 °C [(a), (b), (c), respectively]; 850 °C [(d), (e), (f), respectively]; 900 °C [(g), (h), (i), respectively]; 950 °C [(j), (k), (l), respectively]. The arrow in (b) indicates the location of a Au dot at a NR base/sidewall. The circled region and arrow in (h) indicates a location where secondary VS growth on a VLS grown NR is observed. The circled region and arrow in (k) show a VLS grown NR with a Au particle at the tip.

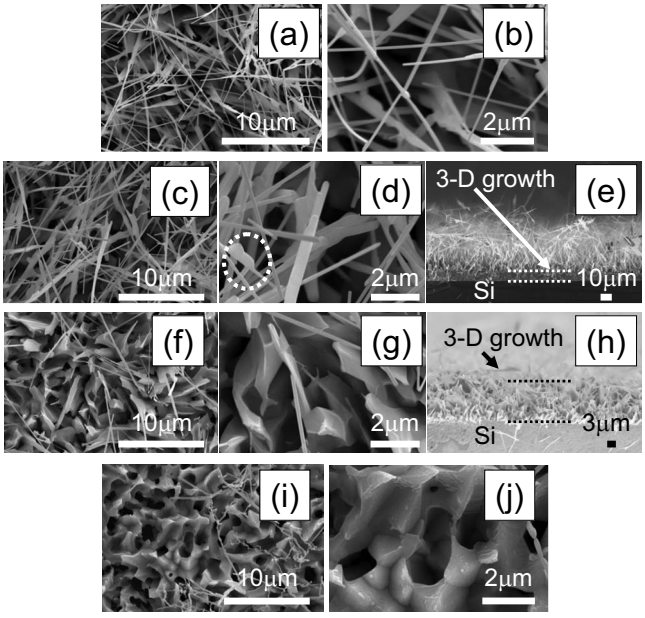

FIG. 2. HR-SEM and SEM images of ZnO nanostructures in plan view at low (5000×) and high magnifications (15 000–30 000×) for samples grown at 1000 °C [(a) and (b), respectively]; 1050 °C [(c) and (d), respectively]; 1100 °C [(f) and (g), respectively]; 1150 °C [(i) and (j), respectively]. Cross-sectional views are shown for samples grown at 1050 °C (e) and 1100 °C (h). The circled region in (d) indicates a location where substantial secondary VS growth on a NR sidewall is observed.

the range of 100–150 nm, some of which are slightly thicker at their bases. The coverage on the substrate (in the Au-coated area) is rather patchy. The NR grows only on the regions initially coated in Au but none of the NR show evidence of Au droplets at their tips. Au particles are seen on NR sidewalls and at bases [Fig. 1(b)]. These NRs display the clear hexagonal faceting characteristic of many ZnO crystals and nanostructures. The growth appears to be solely lengthwise [one-dimensional (1D) growth] along the NR axis and the *c*-section shows the sharp interface between NR and the substrate with no evidence of secondary growth at the NR bases.

Nanostructures grown at 850 °C [Figs. 1(d)–1(f)] also have a NR-like morphology with length in the range of 7–10 μm and diameters around 100–150 nm in the upper portion. The growth at this temperature is more uniform across the entire Au-coated area. None of the NRs show evidence of Au droplets at their tips (although some Au particulates are again observed at the NR sidewalls and at bases, similar to the case of growth at 800 °C) and the upper portions of the NR are hexagonally faceted. It is evident from the SEM top view that many rods show a substantial thickening of the base part due to secondary growth [three dimensional (3D) growth] with diameters in the range of 200–600 nm and this base portion has a length of ~2 μm [Fig. 1(e)]. The *c*-section image [Fig. 1(f)] confirms this observation and crystallites of size about 1 μm in width and 500–700 nm in height are observed at the interface between NR and the substrate.

On increasing the growth temperature to 900 °C we notice some changes in the overall morphology and growth of a fraction of the NR [Figs. 1(g)–1(i)]. Once again we see evidence for hexagonally faceted NR with a constant diameter top portion and thicker faceted bases. The lengths of these NRs are ~10–20 μm. The diameter of the top portion of this NR is ~200 nm. The lower portions have diameters ~400–600 nm. The *c*-section analysis revealed [*c*-section image, Fig. 1(i)] the height of the crystals formed at the substrate interface are increased to 3–4 μm. However, for the first time we see evidence of Au droplets at the top of certain NR and nanostructures, as shown in the higher magnification (dotted circle) portion of Fig. 1(h). NR with Au droplets at their tip present a very different morphology compared to the structures described previously, with no evidence of faceting, and diameters of the order of 500 nm. Most of these NRs show a distinct narrowing at the end to the Au droplet (of diameter ~100 nm). We also see evidence of a combined growth with faceted NR growing out of the tip portion of an unfaceted Au-tipped NR [circled in Fig. 1(h)]. Samples grown at 950 °C [Figs. 1(j)–1(l)], continue this general trend with secondary growth of wall-like features now evident in the top view SEM images. The *c*-section image shows the formation of crystals (height ~4 μm) at the substrate interface. Once again evidence of nanostructures with Au at their tips is seen [indicated by the region in the dotted circle in Fig. 1(k)]. For growth at both 900 and 950 °C the fraction of NR showing Au tips is less than 10%.

Figure 2 shows HR-SEM images displaying top view and magnified top view images of ZnO nanostructures grown at 1000, 1050, 1100, and 1150 °C and also *c*-sections for the samples grown at 1050 and 1100 °C.

Samples grown at 1000 and 1050 °C [Figs. 2(a)–2(e), respectively) show the nanostructures, in general, to be rather long NR/nanowires (>10 μm length). The faceting of the nanostructures is no longer clearly evident. In many cases

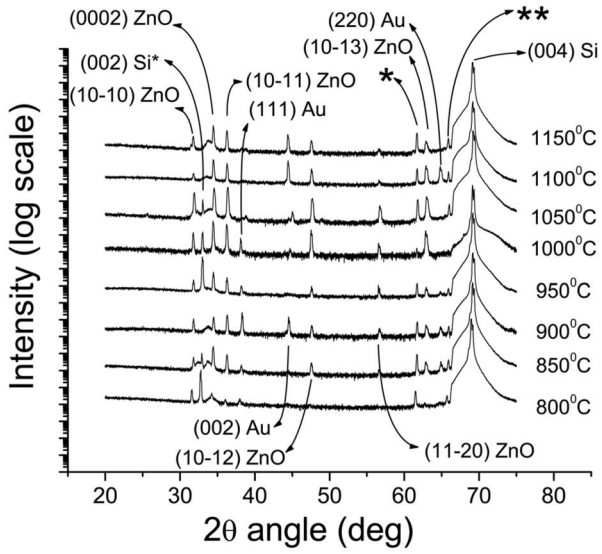

FIG. 3. θ-2θ x-ray diffraction pattern of ZnO nanostructures. Data for different growth temperatures are offset vertically for clarity. The feature marked "(002) Si*" is the nominally forbidden Si (002) reflection, observed due to double diffraction, whose intensity is dependent on the azimuthal angle, ϕ. The feature marked " *" is due to $K\beta$ radiation from the x-ray tube. The feature marked " **" is due to tungsten $L\alpha$ radiation from contamination of the x-ray tube.

the nanostructures show regions of secondary 3D growth on their sidewalls, at various positions along their length, in addition to the 3D growth at the base [e.g., circled region in Fig. 2(d)]. The *c*-section image [Fig. 2(e)] shows that the height of the crystals formed at the substrate interface for the samples grown at 1050 °C has increased to ~8 μm. None of the NR shows evidence of Au droplets at their tips.

Growth at the highest temperatures, 1100 and 1150 °C [Figs. 2(f)–2(j), respectively], shows predominantly 3D foamlike growth morphology (with pore sizes of the order of micron diameter). Few recognizable 1D nanostructures are seen at either growth temperature. The *c*-section image for the sample grown at 1100 °C [Fig. 2(h)] shows that the height of the crystals formed at the substrate interface has increased to ~10 μm. Once again none of the NR shows evidence of Au droplets at their tips.

2. XRD

Figure 3 shows the XRD θ-2θ patterns for ZnO nanostructures grown at temperatures between 800 and 1150 °C. All the observed XRD reflections may be indexed to JCPDS cards for ZnO, Si, or Au.[21] This implies that in all cases the nanostructure phase is wurtzite phase ZnO. The presence of a range of ZnO reflections implies that the ZnO deposit does not show a pronounced texture or alignment, consistent with the SEM images shown above. The XRD patterns indicate the presence of Au in all the samples, though with different reflections dominating at various growth temperatures, and the reflection positions are in all cases equal to those expected for pure Au, within the angular error of the XRD instrument (0.1^0). No evidence is seen for mixed Au–Si or Au–Zn phases in samples grown at any temperature.

3. TEM

Figure 4 shows TEM images of the ZnO sample grown at 950 °C. This sample shows evidence in SEM of NR growth by both the VS and VLS mechanisms and was chosen for TEM analysis on this basis, in order to study both "types" of NR. The fraction of NR with Au tips is rather small in the as-grown samples, and even smaller following preparation of TEM samples since the VLS NR shown in, e.g., Figs. 1(h) and 1(k) are generally of larger diameter than VS NR and thus more physically robust and consequently the ultrasonic TEM preparation procedure tends to remove far more VS NR than VLS NR. However, careful searching has allowed us to locate a region where we could study both types of NR at once, as shown in Fig. 4(a). In both cases the NR grows along the *c*-axis direction (the [0001] direction) of ZnO [as demonstrated by the SAED patterns in Fig. 4(b)]. The SAED pattern reveals that the NR has lattice parameters $a=0.329$ nm and $c=0.524$ nm, which are consistent within the measurement error with the known ZnO lattice parameters of 0.325 and 0.521 nm, respectively.[21,22] The high resolution TEM image in Fig. 4(c) reveals that the ZnO nanostructures sampled here are defect-free and single crystalline. The magnified high resolution TEM image in Fig. 4(d) also shows the (0002) planes of the ZnO NR clearly. EDX data shown in Fig. 4(e) collected on these samples (and a number of others) in the TEM show the NR elemental composition to be ZnO, in agreement with XRD data above.

EDX data from the Au dots on top of the NR [Fig. 5(a)] show only Au peaks and no evidence is seen for Zn or Si incorporation in the Au dots on top of NR.

In all cases where Au drops are seen atop a NR, the interface between the ZnO and the Au is very flat even when viewed in high resolution TEM [HR-TEM, as shown in Fig. 5(b)]. This is suggestive of an epitaxial relationship between the Au drop and the ZnO NR. A SAED pattern of the interface region is shown in Fig. 5(c). A number of extra spots appear, associated with the Au droplet. Based on their displacement from the zone center these have been assigned to Au {111} planes and the interplanar spacings are 0.237 and 0.232 nm for spots labeled "A" and "B," respectively, in excellent agreement with the known value for bulk Au (0.236 nm).[21] However, it has not been possible to deduce a single epitaxial relationship between the Au and ZnO NR. The {111} spot labeled A in Fig. 5(c) indicates that a fraction of the Au crystallite has a ⟨111⟩ axis parallel to the ZnO *c*-axis direction, as generally expected based on matching of the threefold symmetry of the two associated planes, and which has been reported previously.[23] However, the spot labeled B is also associated with a {111} reflection based on its distance from the zone center and the angle, α, it makes to the spot A (124.5°) is not compatible with a single crystalline pattern. In fact the angle between spot B and the ZnO *c*-axis direction implies that a fraction of the Au crystallite has its ⟨100⟩ axis parallel to the ZnO *c*-axis direction also. These results seem to indicate that the Au drops are not single crystalline and that more than one epitaxial relationship to the ZnO may exist in a single drop. This result has not been reported previously, but there are reports in the literature of a variety of epitaxial relationships between Au droplets and

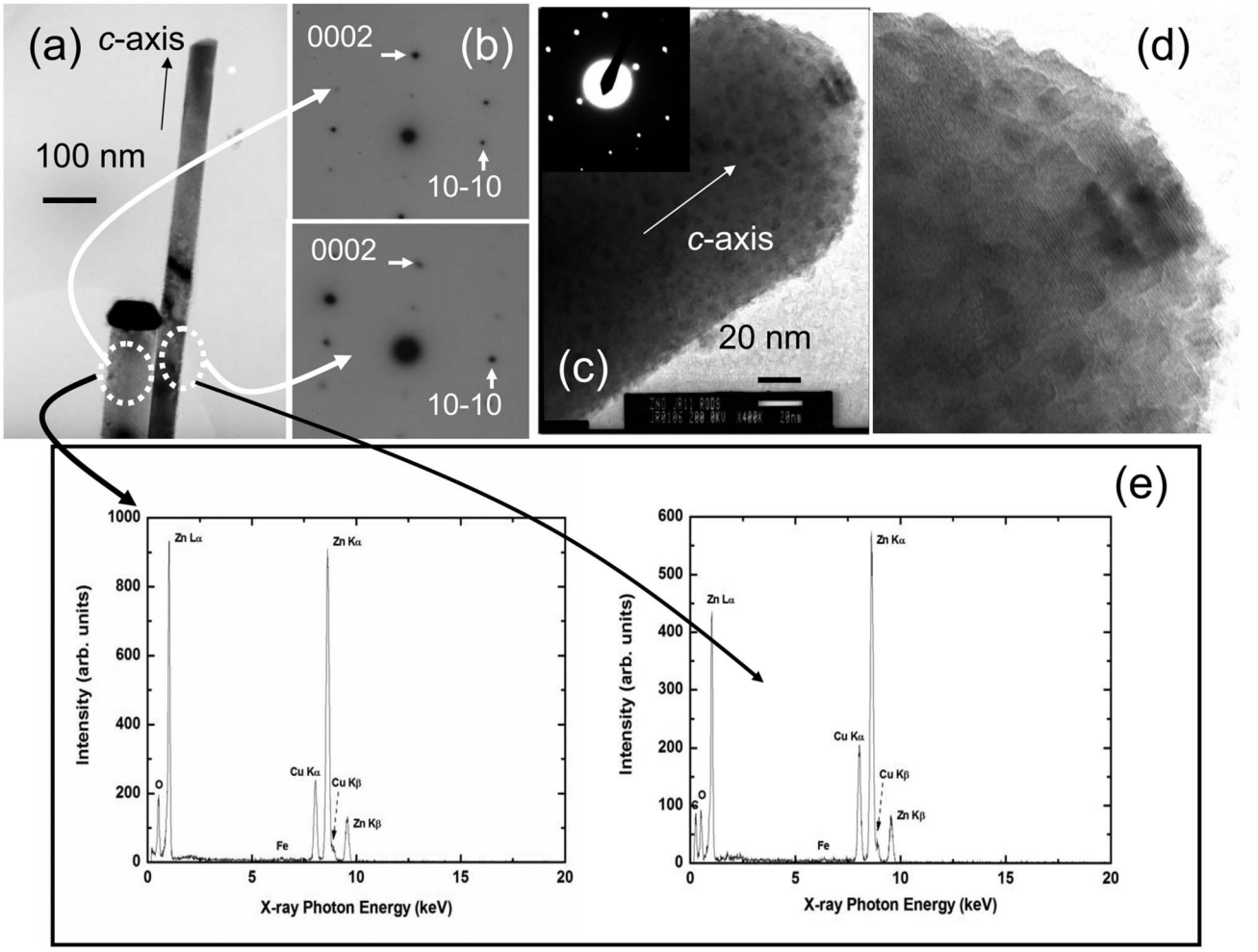

FIG. 4. TEM data from ZnO NR grown at 950 °C. (a) TEM image of VS and VLS grown NRs; (b) SAED pattern of same NR (aperture region indicated in both cases and zone axis in both cases is [1–210]) indicating that the direction of the NR long axis is along the ZnO *c*-axis in both cases; (c) HR-TEM image of VS grown NR (absence of Au at tip is evident) with SAED pattern in inset; (d) magnification of HR-TEM image in (c) showing ZnO (0002) planes; (e) EDX spectra of NR (aperture region indicated in both cases), showing Zn and O compositions. The presence of Cu and small amounts of Fe signal is due to both the Cu TEM grid used to mount the samples and to the electrons striking the chamber walls of the microscope. The very weak peak at ~1.74 keV is associated with Si due to electrons striking SiO_2 from the substrate which adheres to some ZnO NR after the mechanical NR removal process.

VLS grown ZnO NR.[23–25] We have encountered two main difficulties in studying the Au–ZnO epitaxial relationship, specifically; (a) the rather large size and consequent opacity to electrons of the ~100 nm thick Au dots and (b) the low fraction of VLS grown ZnO NR with Au droplets. Due to the consequent scarcity of data we must regard the conclusions above as tentative, and work is continuing to fully understand the nature of the epitaxial relationships between Au droplets and VLS grown ZnO NR.

4. CL and PL

Figure 6(a) shows the CL spectra measured at room temperature for ZnO nanostructures grown at temperatures between 800 and 1100 °C. All the samples show a strong an UV emission band around 3.24 eV attributed to overlapping contributions from free exciton recombination and LO phonon replicas.[26] Little or no emission is seen at longer wavelengths and the weakness/absence of this defect-related emission indicates that the NR are of reasonable optical quality. The significantly lower emission intensity from the sample grown at 800 °C is due primarily to the lower coverage of NR in this sample (the CL comes from an ~1 μm diameter region), but may also be due to some extent to lower crystal quality for this sample, consistent with the lower growth temperature, because a slightly lower emission intensity is also observed for the sample grown at 850 °C where the NR coverage is high. Slight shifts in the UV peak position are most probably associated with surface effects which alter the relative magnitudes of the free exciton and LO phonon contributions to the room temperature emission, as discussed in Ref. 27, because we see no evidence of strain effects in our XRD data.[27]

Figure 6(b) shows low temperature (~18 K) band-edge PL data for samples grown at 950 and 1150 °C. The sample grown at 950 °C shows a dominant bound exciton emission at ~3.356 eV, assigned to the I_9 line associated with In contamination of the source powder.[22] The linewidth of this emission is ~1 meV. The sample grown at 1150 °C shows two dominant bound exciton emission features, the I_9 line once again, in addition to an emission at ~3.360 eV, as-

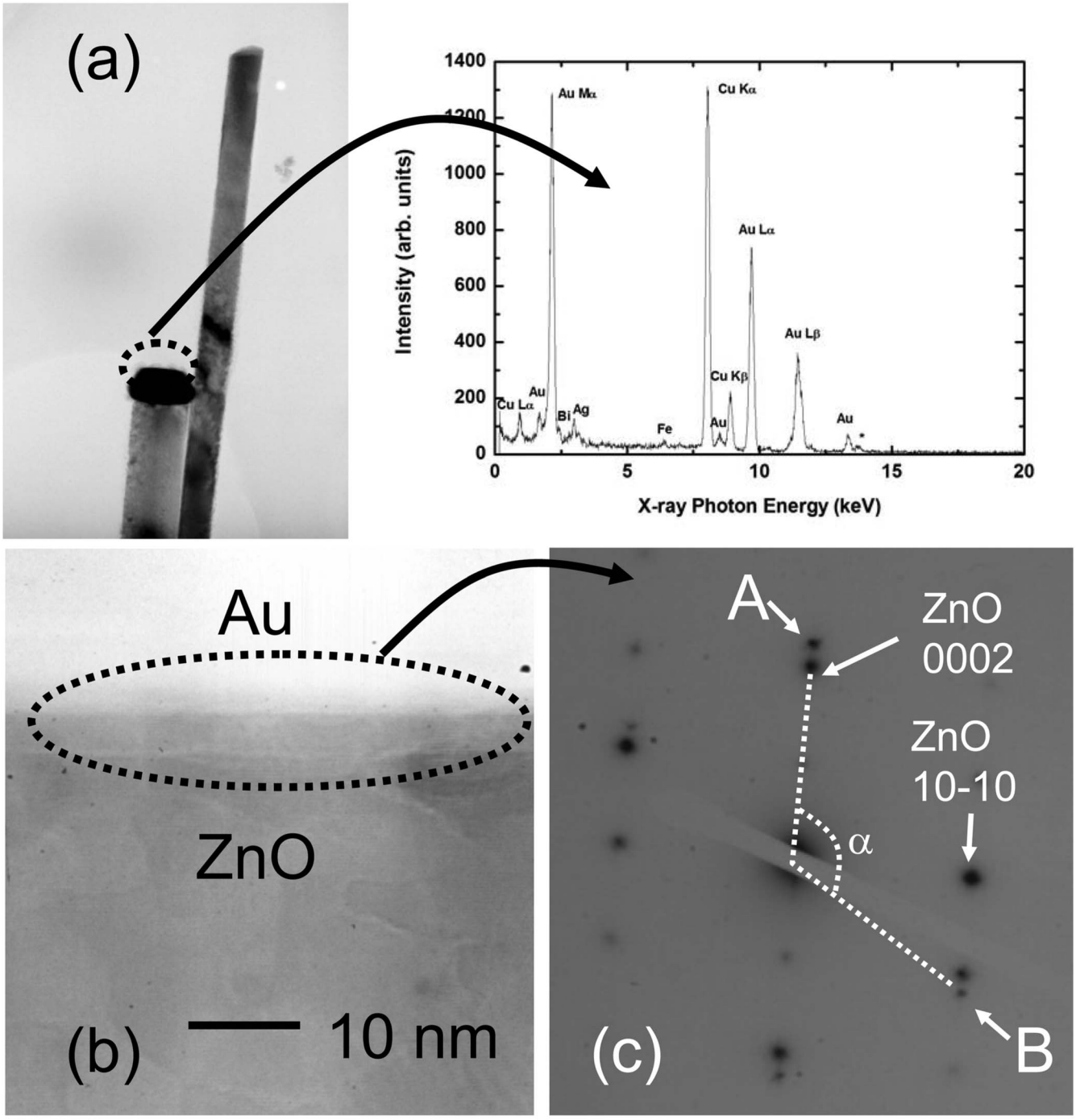

FIG. 5. TEM data from ZnO NR grown at 950 °C. (a) EDX spectrum of Au droplet at top of VLS grown NR (aperture region indicated on left hand side). The presence of Cu and small amounts of Fe signal is due to both the Cu TEM grid used to mount the samples and to the electrons striking the chamber walls of the microscope; (b) HR-TEM image of interface region between ZnO and Au [note contrast reversed compared to (a)]; (c) SAED pattern of region shown in (b).

signed to the I_6 line associated with Al impurities.[28] The presence of this Al-related impurity in samples grown at high temperatures (but not at low temperature growths) is due to contamination by the alumina boat in which the source material is placed, and which can also begin to undergo carbothermal reduction at elevated temperatures, though the large free energy barrier at 1150 °C means that Al is present only in impurity level concentrations.[13] The presence of bound exciton emission and the ability to resolve distinct members of the *I*-series of bound exciton emissions with individual linewidths of the order of 1 meV indicates again that the optical quality of the samples is very good.

B. Discussion: Growth mechanism and morphology

1. Outline of growth mechanism

In broad outline, we propose that the basic growth mechanism proceeds first by the production of Zn vapor through the carbothermal reduction of ZnO powder:[13]

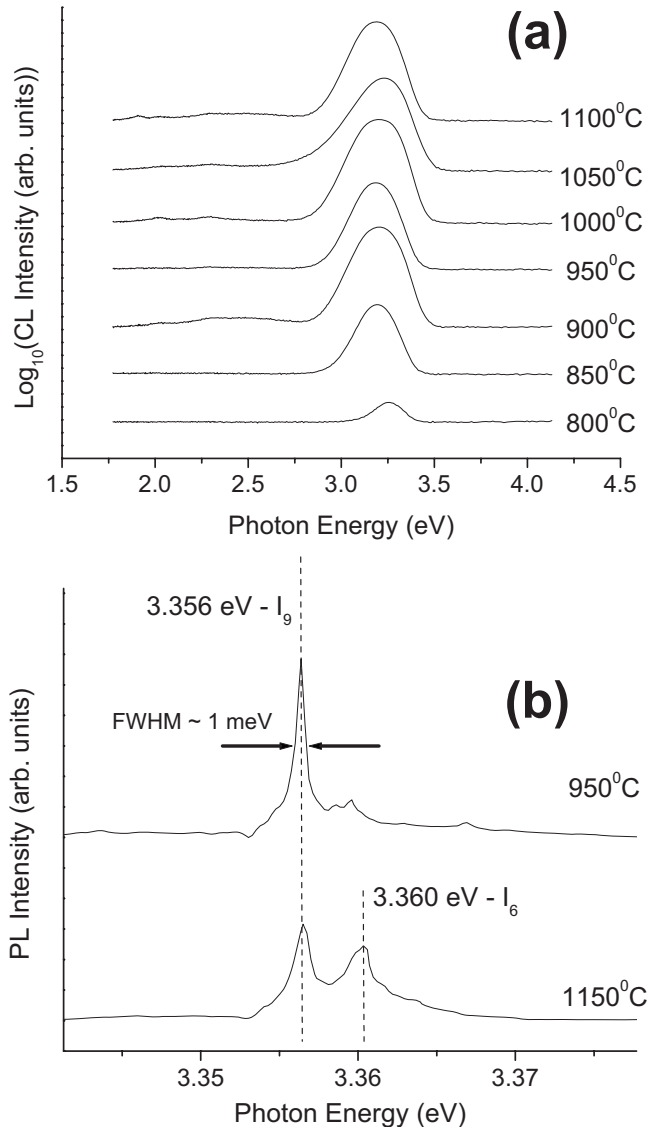

FIG. 6. (a) Room temperature CL data from ZnO nanostructures grown at temperatures between 800 and 1100 °C, in the spectral range of 1.75–4.1 eV, showing only UV band-edge emission. Note that the *y*-axis is a log scale and the individual spectra are offset for clarity. (b) Band edge PL data at ~18 K for samples grown at 950 and 1150 °C. Note that the spectra are offset for clarity.

$$\mathrm{ZnO} + C \rightarrow \mathrm{Zn} + \mathrm{CO}. \quad (1)$$

The Zn vapor atoms then impinge on and stick to the Au-catalyzed regions of the substrate (which provide preferential accommodation sites) and dwell for a period. At all temperatures the Zn may react directly with the residual oxygen in the growth tube to form ZnO nuclei. These nuclei then provide further accommodation sites for Zn vapor atoms, in addition to the Au catalyst, and the nanostructures evolve via the VS mechanism. We note that a number of authors refer to the growth of ZnO nanostructures via Zn vapor deposition and oxidation as self-catalyzed VLS growth, where subnanometer Zn clusters are observed at the growth front.[29] This terminology may also be applied to the subsequent growth, following nucleation, of the majority of ZnO nanostructures in our system as described above. Indeed for our experiments, where no evidence of large Zn droplets is seen atop NR (consistent with the low Zn vapor supersaturation values mentioned in Sec. II above), it does not appear that a very clear distinction can be made between the self-catalyzed VLS growth mechanism described in Ref. 29 and traditional VS growth. This is in contrast to self-catalyzed VLS growth of SnO_2 nanostructures reported in the literature, where clear evidence is seen for large Sn droplets atop SnO_2 nanostructures.[30] We thus continue to use the term VS growth to describe this growth mode in our system while noting the similarities to self-catalyzed VLS growth discussed above. In addition to VS growth, within a certain temperature range the Zn vapor may also condense on and dissolve in the Au and growth continues via the Au-catalyzed VLS mechanism, in parallel with the VS growth route described above.

The first part of the proposed growth mechanism, i.e., Zn impingement and sticking to the surface followed by oxidation, rather than a gas phase Zn–O reaction followed by condensation of gas phase ZnO or ZnO_x molecules, is supported by various studies in the literature of the congruent sublimation of ZnO,. These show that molecular ZnO is nearly always below the detection limit.[31,32] These experimental findings are also supported by thermochemical data for the gas phase reaction of Zn with O_2, which show Gibb's free energy is positive (of the order of 115–125 $\mathrm{kJ/mol_{(Zn)}}$) at the temperatures in question which means that the gas phase ZnO vapor pressures are $\sim 10^{-6}$–10^{-5} times less than the Zn vapor pressures.[17] Therefore condensation of gas phase ZnO is unlikely to contribute to ZnO nanostructure growth unless the sticking coefficients for Zn on the substrate are very low (which is not the case on the Au coated regions as discussed below), and even then the growth rates will be very small. The reaction of the oxygen with Zn atoms that have impinged and stuck to the Au-catalyzed regions is facilitated by the reduction in the entropy (and increase in free energy) of the Zn atoms while stuck to the substrate compared to their existence in the gas phase, promoting the oxidation reaction. There is no evidence that the Au has any catalytic effect on this reaction, however. The oxidation rate is temperature dependent with an activation energy of 0.73 eV.[33] The initial part of the growth may also lead to reaction of the Zn atoms with the SiO_2 layer on the substrate surface to form nanoscale zinc silicate islands. This effect has been observed by Lim *et al.*,[12] but our data in Sec. III B 5 below indicate that this is not a crucial aspect of the growth. The latter part of the proposed growth mechanism, the oxidation of Zn by the residual oxygen in the growth tube, has been tested by flushing the growth tube for 45 min prior to growth, rather than our customary 10 min flushing time. Experiments performed using this longer flushing time show no evidence of ZnO growth on Au-catalyzed substrates for temperatures less than 1100 °C. For temperatures at and above 1100 °C, a very small amount of growth is seen on the Au-coated regions due to direct sublimation of a fraction of the ZnO powder, creating Zn vapor and O_2 directly.[31] In our experiments the oxygen content of the growth chamber was not varied and hence the variation in growth mechanism and morphology is due to variations in the Zn vapor content and we concentrate our attention on this aspect below.

In the case of bare Si substrates (i.e., no Au coating), we observe no evidence of ZnO nanostructure growth at any of the temperatures studied. In our experiments the bare Si surface is covered with a native SiO_2 layer. The absence of ZnO growth on bare regions of the substrate is explained by the low sticking coefficient of Zn on SiO_2.[34,35] In contrast, the Au-coated regions of the substrate provide energetically favorable regions for Zn atom to be accommodated with a high sticking coefficient.[24] The fact that ZnO structures provide nucleation sites for Zn vapor and thus VS growth is demonstrated by a number of incidences of secondary nucleation of ZnO nanostructures on previously grown structures, such as that shown in the circled region of Fig. 1(h).

2. 800–850 °C growth temperatures

While growth of ZnO nanostructures on Au-coated Si has generally been attributed to the VLS growth mechanism in the literature[9,36] the VLS mechanism requires that Au droplets be found on the tips of the NR. Figures 1(a)–1(f) show that there are no Au droplets on the NR tips grown at 800 and 850 °C indicating that the growth is via the VS growth mechanism. The same inconsistency has been highlighted recently by a number of other reports in the literature.[11,12] The growth at these lower temperatures in our system is due entirely to VS growth, and this is demonstrated by the hexagonally faceted morphology and flat NR tops observed in SEM, which are also seen for growth on ZnO buffer layers with no Au catalyst.[5]

The absence of VLS growth at this temperature may be explained by considering the phase diagram for a Au–Zn alloy.[37] A liquid Au–Zn alloy will form at 800–850 °C for atomic Zn percentages in the range of 17%–13%. Given the likely low Zn vapor density values at these growth temperatures (considering the energetics of the Ellingham diagram describing the carbothermal reduction reaction[13,16,17]) and the low temperatures for diffusion of Zn into Au it is unlikely that such a concentration can be established in the Au particulates, as the Zn atoms impinging at a relatively low rate on the Au will tend to oxidize before they can be incorporated into the Au to form an alloy and thus the VLS mechanism cannot operate. One other possible explanation for the absence of Au droplets at the tips of NR is that the NR grows by the VLS mechanism but that, in many cases, the Au tips were mechanically displaced from the NR during growth. We can rule out this possibility based on the discussion below in relation to Fig. 7.

The low density of the NR for growth at 800 °C is due to the low Zn pressure at the low growth temperatures, and this increases with increasing growth temperatures, as the flux of Zn atoms from the vapor increases and more ZnO nuclei form. The thickening of the bases and the development of 3D morphology at the NR bases discussed in Sec. III A is associated with secondary growth, mentioned in relation to the discussion of some features in Fig. 1(h). Following initial nucleation of ZnO crystals, subsequent growth initially takes place predominantly along the [0001] direction, which is the normal case for ZnO as the sticking coefficient of Zn atoms to this face is the highest compared to other ZnO faces[38] and thus the primary growth mode will be a 1D

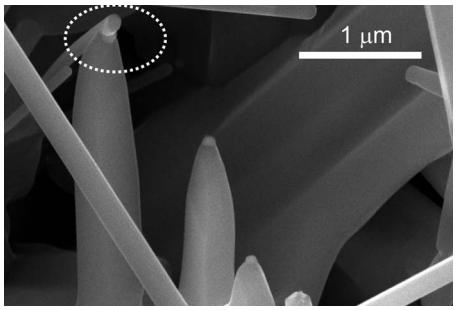

FIG. 7. HR-SEM image of sample grown at 900 °C. The circled region shows an example where a VS NR pierces the Au tip of a VLS NR and the Au tip is not displaced from the top of the VLS NR, demonstrating the mechanical stablility of the Au catalyst drops on VLS NR against perturbations.

growth along the [0001] direction and the length of the NR will increase with increasing growth temperature due to the increasing flux of Zn atoms, as observed in our data. However growth will also occur to some extent on other ZnO faces after the ZnO NR nucleate and begin to grow, though with lower growth rates due to the reduced sticking coefficients on these ZnO faces.[38] This will mainly lead to a gradual thickening of the bases over the period of the growth. This secondary growth occurs mainly at the bases because (a) the base regions are the regions longest in existence and thus naturally they show the greatest degree of growth off the [0001] direction and (b) sidewall nucleation at the base of a NR is enhanced by the presence of both the existing NR sidewall and neighboring Au particulates which will increase the sticking coefficient. As long as the thickened base regions do not coalesce secondary growth off the [0001] direction is relatively slow.

3. 900–950 °C growth temperatures

As the growth temperature rises to the 900–950 °C range, a number of the NRs are observed to have Au droplets at their tips, and these NRs show an unfaceted appearance and generally larger diameter than faceted NR. We believe that these NRs are grown by a "genuine" Au-catalyzed VLS process, facilitated by the higher Zn vapor pressure in combination with the lower atomic Zn percentages required to form a liquid alloy in the 900–950 °C range. The percentage yield of VLS NR is $<10\%$ at both 900 and 950 °C. The small relative yield of VLS NR is most likely due to the rather thin Au catalyst layers used initially.

The XRD data shown in Fig. 3 show the presence of Au in the samples grown in this temperature range and in all cases the reflections occur at positions consistent with those of pure Au, and show no evidence of being due to a Au–Zn alloy. EDX data collected with the TEM (shown in Fig. 5) corroborate the fact that only pure Au was detected when probing the Au particulates. The phase diagram for the Au–Zn system predicts that Zn remains soluble in Au for Zn atomic percentages $<10\%$ down to room temperature and therefore that one might see a change in lattice constant associated with such alloying. However, the oxygen rich atmosphere in which growth occurs will alter the energetics of this phase diagram and we believe that as the temperature

drops Zn will precipitate out of solution and oxidize to form ZnO, leaving only pure Au behind at the VLS NR tips. This final precipitation of Zn out of the droplet to form ZnO as the system cools may be the reason for the tapered end portions seen on many VLS NRs, such as those in Fig. 1(h). These effects (precipitation of Zn out of cooling NR and consequent tapering of the ends of NR) have previously been reported for the behavior of Ga in the growth of GaAs NR in As-rich and As-deficient environments and our observations support the mechanism proposed in that report.[39]

The absence of Si signals in the EDX data of Au tips on top of VLS NR strongly implies that alloying with Si/SiO_2 is not required for VLS NR growth. If Si were incorporated at high temperature growth and precipitated out (and oxidized) as the system cooled (as predicted by the Au–Si phase diagram[37]), one would expect to observe a Si/SiO_2 shell or similar Si-composed deposit close to the NR Au tip. Even if the phase diagram is more complicated due to the presence of Au, Si, Zn, and O, alloying of Au with Si should still lead to observable Au EDX signals in Au tips postgrowth, and none are seen.

The Au droplets at the VLS NR tips appear to be quite mechanically stable against perturbations and we have even observed situations where VS NR "pierce" the Au tips of VLS NR, and the Au tips are not displaced from the top of the VLS NR. An example of this is shown in Fig. 7. In the 900–950 °C range, both the VS and VLS mechanisms operate at the same time, and as indicated above Zn atoms may impinge on and stick to ZnO nuclei in addition to the Au regions of the substrate. A pronounced example of secondary growth of a VS NR growing from a VLS NR is shown in Fig. 1(h).

There is no evidence that Au is consumed during VLS growth of ZnO nanowires (by incorporation into growing NR or onto the NR surfaces), with VLS growth terminating after the Au dot has been consumed. This is shown by careful EDX measurements made along many different NRs (including those with and without Au dots atop them) which in all cases show no detectable Au signal [see Fig. 4(e)].

4. 1000–1150 °C growth temperatures

For growth temperatures at and above 1000 °C, there is no further evidence of VLS growth and the faceting effects of the NR are less evident. Long NRs are observed in addition to increased rates of secondary growth, particularly at the NR bases and occasionally at random locations along the NR walls. The same general growth mechanism of Zn atom impingement from the vapor will be expected to apply at these temperatures. This leads to the longer NR growth in the first instance. The absence of VLS growth in our experiments at these temperatures is surprising, as both the Zn vapor density is quite high in this temperature regime and the Au nanoparticles should easily melt to incorporate Zn into an alloy. The presence of characteristic x-ray reflections associated with Au in Fig. 3 is seen at all temperatures up to 1150 °C which indicates that the Au is not evaporating from the substrates and therefore is unlikely to evaporate from the NR tips. We propose that at these higher temperatures the sticking coefficient and dwell time of the impinging Zn atoms on Au reduces and the oxidation rate of Zn atoms increases [determined by a rate constant with activation energy 0.73 eV (Ref. 33) and that these effects combine to reduce the efficiency of incorporation of Zn into a Au–Zn alloy so that ZnO nuclei form preferentially by the VS mechanism once again. To the best of our knowledge there has been no discussion in the ZnO nanostructure literature of the temperature dependence of the oxidation reaction, and we believe this must be important in determining the nature of the nanostructure growth mechanism, i.e., between VS and VLS growth.

Our data in Fig. 2 also show that at higher temperatures secondary growth on the non-(0001) faces increases substantially. We attribute this to the combined effects of increased oxidation rate and coalescence of the thickened and randomly aligned NR bases. As the growth temperature, and thus the Zn vapor density and oxidation rate increase, the rate of secondary, 3D, growth at NR bases and elsewhere will increase. The bases will ultimately coalesce before the end of the growth period. As the bases coalesce, the locations at which the crystals meet will provide highly energetically favorable sites for Zn atom capture, as the unaligned crystals will meet at a range of angles and form grain boundaries with a high degree of lattice imperfection, broken bonds, step edges, etc. At this stage, secondary growth will begin to dominate the overall growth process as the sticking coefficient of Zn vapor atoms to these imperfect regions will be greater than to the flat prismatic and mixed polarity ZnO faces.[40] Thus at the very highest temperatures the secondary, 3D growth begins to dominate and the NR are "swallowed up" by the 3D growth to yield the highly porous structures seen for growths at 1100 and 1150 °C. The absence of clear faceting along the NR (where identifiable individual NR are present e.g., at growth temperatures of 1000 and 1050 °C) is also due to random nucleation of secondary growth sites due to the high Zn vapor density and oxidation rates at these temperatures. An example of these effects is seen in Fig. 2(d).

5. Comparison of growth on Au covered Si with thick oxide layers

We have stated above that a number of previous reports have uniformly attributed growth of ZnO nanostructures on Au-catalyzed Si to the VLS mechanism, and we have presented our arguments against this uniform attribution. More recent reports have also commented on the inconsistencies in this uniform attribution in a similar vein to the current work.[11] The report in Ref. 11 has suggested growth mechanisms relying on alloying between Si atoms in the substrate and the Au catalyst. Our EDX data provide strong evidence against such a proposed mechanism, as discussed in Sec. III B 3 above, and we have attempted to further test the applicability of this model to our growth conditions by growing on Si samples with thick SiO_2 layers (~ 3 μm thick) where the direct alloying of Au and Si by diffusion is unlikely due to the thick barrier layer which is far greater than typical native oxide thicknesses (<5 nm).

We have conducted an identical series of growth at all temperatures on these thick SiO_2 layers, and identical results

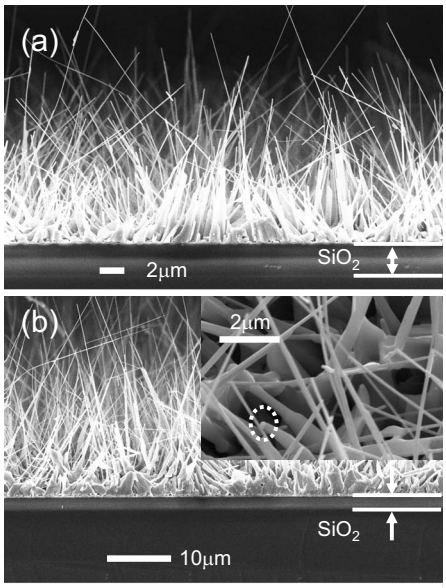

FIG. 8. Cross-sectional SEM images of samples grown on 3 μm thick SiO_2 layers at (a) 850 °C and (b) 950 °C. The inset of (b) shows evidence (circled) for VLS grown NR in samples grown on 3 μm thick SiO_2 layers at 950 °C.

to those displayed in Figs. 1 and 2 are found, including the presence of VLS grown NR at low percentage yields only for growth at 900 and 950 °C [see inset of Fig. 8(b)]. Cross-sectional SEM data on these samples are shown in Fig. 8 (for samples grown at 850 and 950 °C). In both cases no evidence is seen of any significant disturbance/breaching of the thick oxide layers at regions where ZnO nanostructures are grown. This is consistent with the lack of evidence for the presence of Si either in, or close to, the Au tips of VLS NR seen in the EDX data of Au caps shown in Fig. 5 for growth on native oxide layers. EDX data (not shown) of Au tips on VLS NR grown on thick SiO_2 layers also display no evidence of Si. These data in their entirety indicate that the growth model involving alloying between Si atoms in the substrate and the Au catalyst[11,41] is not consistent with our data. The data shown in Ref. 12 are consistent with our results, particularly in the case where graphite powder was used for the carbothermal reduction, which is similar to our growth reaction and we cannot rule out the possibility of a reaction between the Zn atoms and the SiO_2 layer to form nanoscale zinc silicate islands as part of the initial NR nucleation process. Our data are also consistent with the report in Ref. 35.

IV. CONCLUSIONS

We have studied the growth of ZnO nanostructures on Au-catalyzed Si substrates in the temperature range of 800–1150 °C. A wide variation in morphology is seen in SEM, from high aspect 1D NR growth at low and intermediate temperatures to a porous 3D morphology at the highest growth temperatures. The structural properties as revealed by TEM show that individual NR are single crystalline and free of defects such as twin boundaries and dislocations. The NR long axis is parallel to the ZnO *c*-axis direction. PL studies show UV excitonic emission and no evidence of deep level emission. The growth mechanism is VS at both low and high temperatures, and genuine VLS growth is seen only in a narrow temperature band (900–950 °C)

We have proposed a simple growth model based on the impingement and sticking of Zn atoms solely at the Au covered regions of the substrate initially, followed either by direct oxidation to yield VS growth or formation of a Au–Zn alloy followed by precipitation and oxidation (VLS) growth. This simple model accounts for the wide range of observed morphologies and successfully explains the main features seen in all our samples. We have also discussed the origin of the narrow temperature band in which VLS growth is observed based on a lack of sufficient Zn supply combined with insufficient thermal energy to enable Zn to diffuse into the Au to maintain a Au–Zn alloy at low temperatures and reduced efficiency of incorporation of Zn into an alloy at higher temperatures due to shorter dwell times and higher oxidation rates. The potential effects of the Zn oxidation reaction and the associated activation energy for this process, which are aspects heretofore little mentioned, on the growth morphologies have been discussed also. We have studied growth on thick SiO_2 layers and found identical results to those on native oxide layers indicating that growth models in the literature involving alloying between Si atoms in the substrate and the Au catalyst are not consistent with our data.

Our data show that it is possible to reproducibly control the morphology of ZnO nanostructures from high aspect ratio NR to porous nanostructures by simply varying the growth temperature in a simple growth method. This morphology control via one parameter control using a simple growth technique, and the understanding of the growth mechanisms which underlie it, should enable reliable commercial fabrication of ZnO nanostructures with various applicable morphologies.

ACKNOWLEDGMENTS

We acknowledge financial support from the Science Foundation Ireland (Investigator Grant No. 02/IN1/I95 and RFP Grant No. 06/RFP/PHY052) and the Irish Higher Education Authority under the NDP. We are grateful to Mr. Conor McLoughlin for his assistance during the course of this study.

[1] M. H. Huang, S. Mao, H. Feich, H. Yan, Y. Wu, H. Kind, E. Weber, R. Russo, and P. Yang, Science **292**, 1897 (2001).
[2] C. X. Xu and X. W. Sun, Appl. Phys. Lett. **83**, 3806 (2003).
[3] W. Hughes and Z. L. Wang, Appl. Phys. Lett. **82**, 2886 (2003).
[4] E. Comini, G. Faglia, G. Sberveglieri, Z. W. Pan, and Z. L. Wang, Appl. Phys. Lett. **81**, 1869 (2002).
[5] R. T. Rajendra Kumar, E. McGlynn, C. McLoughlin, S. Chakrabarti, R. C. Smith, J. D. Carey, J. P. Mosnier, and M. O. Henry, Nanotechnology **18**, 215704 (2007).
[6] J. J. Wu and S. C. Liu, Adv. Mater. (Weinheim, Ger.) **14**, 215 (2002).
[7] W. I. Park, G. Yi, M. Kim, and S. L. Pennycook, Adv. Mater. (Weinheim, Ger.) **14**, 1841 (2002).
[8] Z. Zhong, D. Wang, Y. Cui, M. W. Bockrath, and C. M. Leiber, Science **302**, 1377 (2003).
[9] M. H. Huang, Y. Y. Yu, H. Feick, N. Tran, E. Weber, and P. D. Yang, Adv. Mater. (Weinheim, Ger.) **13**, 113 (2001).
[10] A. P. Levitt, *Whisker Technology* (Wiley, New York, 1971).
[11] Y. J. Li, M. Feneberg, A. Reiser, M. Schirra, R. Enchelmaier, A. Ladenburger, A. Langlois, R. Sauer, and K. Thonke, J. Appl. Phys. **99**, 054307 (2006).

[12]Y. S. Lim, J. W. Park, M. S. Kim, and J. Kim, Appl. Surf. Sci. **253**, 1601 (2006).
[13]H. J. T. Ellingham, J. Soc. Chem. Ind., London **63**, 125 (1944).
[14]W. L. Hughes and Z. L. Wang, J. Am. Chem. Soc. **126**, 6703 (2004).
[15]C. Ye, X. Fang, Y. Hao, X. Teng, and L. Zhang, J. Phys. Chem. B **109**, 19758 (2005).
[16]P. W. Atkins, *Physical Chemistry*, 4th ed. (Oxford University Press, New York, 1992).
[17]IVTANTHERMO for Windows, 1992–2008, Thermochemical Database, Russian Academy of Sciences.
[18]*Handbook of Chemistry and Physics*, 74th ed., edited by D. R. Lide (CRC, Boca Raton, 1993).
[19]R. T. Rajendra Kumar, J. Grabowska, J. P. Mosnier, M. O. Henry, and E. McGlynn, Superlattices Microstruct. **42**, 337 (2007).
[20]H. M. Cheng, H. C. Hsu, S. Yang, C. Y. Wu, Y. C. Lee, L. J. Lin, and W. F. Hsieh, Nanotechnology **16**, 2882 (2005).
[21]ZnO: JCPDS Card No. 36-1451; Si: JCPDS Card No. 27-1402; Au: JCPDS Card No. 04-0784 (unpublished).
[22]Ü. Özgür, Ya. I. Alivov, C. Liu, A. Teke, M. A. Reshchikov, S. Dogan, V. Avrutin, S.-J. Cho, and H. Morkoç, J. Appl. Phys. **98**, 041301 (2005).
[23]M. Kirkham, X. D. Wang, Z. L. Wang, and R. L. Snyder, Nanotechnology **18**, 365304 (2007).
[24]C. Borchers, S. Muller, D. Stichtenoth, D. Schwen, and C. Ronning, J. Phys. Chem. B **110**, 1656 (2006).
[25]C. L. Wu, L. Chang, H. G. Chen, C. W. Lin, T. F. Chang, Y. C. Chao, and J. K. Yan, Thin Solid Films **498**, 137 (2006).
[26]L. J. Wang and N. C. Giles, J. Appl. Phys. **94**, 973 (2003).
[27]T. Voss, C. Bekeny, L. Wischmeier, H. Gafsi, S. Börner, W. Schade, A. C. Mofor, A. Bakin, and A. Waag, Appl. Phys. Lett. **89**, 182107 (2006).
[28]B. K. Meyer, H. Alves, D. M. Hofmann, W. Kriegseis, D. Forster, F. Bertram, J. Christen, A. Hoffmann, M. Strassburg, M. Dworzak, U. Haboeck, and A. V. Rodina, Phys. Status Solidi B **241**, 231 (2004).
[29]Z. L. Wang, X. Y. Kong, and J. M. Zuo, Phys. Rev. Lett. **91**, 185502 (2003).
[30]Y. X. Chen, L. J. Campbell, and W. L. Zhou, J. Cryst. Growth **270**, 505 (2004).
[31]A. V. Makarov, S. G. Zbezhneva, V. V. Kovalenko, and M. N. Rumyantseva, Inorg. Mater. **39**, 594 (2003); Neorg. Mater. **39**, 705 (2003).
[32]L. Brewer, Chem. Rev. (Washington, D.C.) **52**, 1 (1953).
[33]O. E. Kashireninov, G. B. Manelis, and L. F. Repka, Zh. Fiz. Khim. **56**, 1030 (1982) [Russ. J. Phys. Chem. **56**, 630 (1982)].
[34]S. W. Kim, T. Kotani, M. Ueda, S. Fujita, and S. Fujita, Appl. Phys. Lett. **83**, 3593 (2003).
[35]D. Zhao, C. Andreazza, P. Andreazza, J. Ma, Y. Liu, and D. Shen, Chem. Phys. Lett. **399**, 522 (2004).
[36]P. D. Yang, H. Q. Yan, S. Mao, R. Russo, J. Johnson, R. Saykally, N. Morris, J. Pham, R. G. He, and H. J. Choi, Adv. Funct. Mater. **12**, 323 (2002).
[37]*Binary Alloy Phase Diagrams*, edited by T. B. Massalski (ASM, Metals Park, OH, 1990).
[38]H. Kato, M. Sano, K. Miyamoto, and T. Yao, Jpn. J. Appl. Phys., Part 2 **42**, L1002 (2003).
[39]A. I. Persson, M. W. Larsson, S. Stenström, B. J. Ohlsson, L. Samuelson, and L. R. Wallenberg, Nature Mater. **3**, 677 (2004).
[40]A. Pimpinelli and J. Villain, *Physics of Crystal Growth* (Cambridge University Press, Cambridge, 1998).
[41]C. Y. Lee, T. Y. Tseng, S. Y. Li, and P. Lin, Tamkang J. Sci. Eng. **6**, 127 (2003).